Enhancement of Internal Motions of Lysozyme through Interaction with Gold Nanoclusters and its Optical Imaging

ARTICLE *in* THE JOURNAL OF PHYSICAL CHEMISTRY C · DECEMBER 2014

Impact Factor: 4.77 · DOI: 10.1021/jp508582c

8 AUTHORS, INCLUDING:

Vijaya Sundar
Central Leather Research Institute
9 PUBLICATIONS **29** CITATIONS
SEE PROFILE

Morten N. Pedersen
University of Southern Denmark
7 PUBLICATIONS **23** CITATIONS
SEE PROFILE

Natarajan Arul Murugan
KTH Royal Institute of Technology
72 PUBLICATIONS **576** CITATIONS
SEE PROFILE

Hans Agren
KTH Royal Institute of Technology
867 PUBLICATIONS **18,824** CITATIONS
SEE PROFILE

THE JOURNAL OF PHYSICAL CHEMISTRY C

Article

pubs.acs.org/JPCC

Enhancement of Internal Motions of Lysozyme through Interaction with Gold Nanoclusters and its Optical Imaging

S. K. Mudedla,[†,‡] E. R. Azhagiya Singam,[†] J. Vijay Sundar,[†] Morten N. Pedersen,[§] N. Arul Murugan,[∥] Jacob Kongsted,[§] Hans Ågren,[∥] and V. Subramanian*[,†,‡]

[†]Chemical Laboratory, CSIR-Central Leather Research Institute, Adyar, Chennai-600 020, India

[‡]Academy of Scientific and Innovative Research (AcSIR), Anusandhan Bhawan, 2 Rafi Marg, New Delhi 110 001, India

[§]Department of Physics, Chemistry and Pharmacy, University of Southern Denmark, Campusvej 55, 5230 Odense M, Denmark

[∥]Division of Theoretical Chemistry and Biology, School of Biotechnology, Royal Institute of Technology, SE-106 19 Stockholm, Sweden

Supporting Information

ABSTRACT: Understanding the interaction of gold nanoclusters with proteins has important ramifications in various fields. We present a study of the interaction between gold nanoclusters and lysozyme investigated using classical molecular dynamics and center-of-mass pulling simulations. The results reveal that the gold nanoclusters induce significant structural changes in lysozyme. Because the internal motions of lysozyme are related to its function, the changes in these internal motions have been quantified using principal component analysis of the molecular dynamics trajectories. The internal motions of lysozyme that are important for its function have been altered because of the interaction with the gold nanocluster. We have also explored how these induced changes in the lysozyme structure affect specific optical properties of the gold nanocluster using the complex polarization propagator method within the time-dependent density functional theory framework, which is of relevance for studies of the optical imaging of lysozyme using gold nanoclusters as molecular probes.

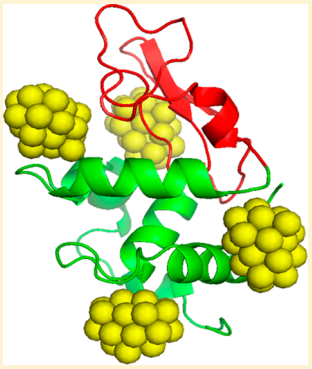

INTRODUCTION

Gold nanoclusters (AuNCs) represent an attractive new class of materials in nanotechnology because of their size- and shape-dependent quantum behavior as well as remarkable optical and catalytical properties. These are also referred to as clusters, quantum confined or sized clusters, metal quantum dots, quantum clusters, and super atoms.[1−16] The AuNCs have been found to be highly useful in bioimaging and biosensing applications.[17,18] The surface plasmon absorption is an important property of luminescent gold nanoparticles, and it can be tuned by changing the size of the particles. On the basis of this property, luminescent gold nanoparticles have been classified into two categories: (i) molecular nanoparticles (0.3−3 nm) and (ii) plasmonic nanoparticles (>3 nm). When the size of the gold nanoparticle is within the range from 0.3 to 3 nm, the surface plasmon absorption was not observed and they showed distinct absorption features in contrast to the gold nanoparticles. The molecular nanoparticles within the 0.3−3 nm range are divided into two categories based on their core size: (i) a few atom gold nanocluster (AuNCs) (0.3 to 1 nm) and (ii) a few nanometer gold nanoparticle (1 to 3 nm).[19]

DNA-functionalized and DNA-linked gold nanoparticles have unique optical, thermodynamic, and structural properties.[20−22] These hybrid systems have been used to detect DNA and proteins. Hence, the properties of these composites have become popular targets for modeling studies. For example, molecular dynamics simulations have been conducted to understand the interaction of double-strand and single-strand DNA with gold clusters and gold surfaces.[23,24] Furthermore, bare AuNCs have been used to immobilize proteins so that the proteins can be uniformly tethered on its surface with a view to developing new biochips.[25] The immobilization of proteins such as green fluorescent proteins and human oncostatin-M on the surface of gold clusters have been extensively studied using atomic force microscopy and molecular surface area analysis.[26] The immobilization of proteins on AuNCs has been achieved through the formation of a gold−thiol bond between AuNCs and cysteine, which is present on the surface of the protein.[26] In addition to the gold−thiol bond, the AuNCs can also be stabilized by the nearby amino acids through noncovalent interactions. The proteins which do not have cysteine on their surface interact through a noncovalent interaction with AuNCs. The green fluorescent protein does not have the cysteine on the surface; therefore, the interaction between AuNCs protein occurs through noncovalent interactions.[27] Monolayer protected AuNCs and bare colloidal gold nanoparticles have also been found to be useful for site-specific labeling of proteins.[28] Furthermore, AuNCs have been synthesized in the protein milieu,[29−34] and lysozyme has been used to prepare red-emitting Au_{25} clusters, which are highly sensitive toward toxic mercury(II)

Received: August 25, 2014
Revised: November 19, 2014

   dx.doi.org/10.1021/jp508582c | J. Phys. Chem. C XXXX, XXX, XXX−XXX

ions.[35] The biological activity of lysozyme was retained on the formation of AuNCs;[36] for instance, AuNCs encapsulated lysozymes have been demonstrated to act as antimicrobacterial agents.[37] Pradeep and co-workers have shown that the lysozyme wraps the Au_{10} or Au_{12} clusters by the formation of Au−S bond. The growth of the cluster is facilitated by the breaking of disulfide bonds. Significant decrease in the helical content of lysozyme has been observed because of the breakage of disulfide bonds.[38] The AuNCs in the protein milieu are stabilized through the formation of either S−Au−S−Au−S staples or Au−S bonds between cysteine and gold atoms.[39] In addition to Au−S, AuNCs can also be protected by the noncovalent interaction with the surrounding amino acids.

Previous studies have shown that it is possible to synthesize fluorescent Au_{25} clusters using insulin.[40] The biological activity of insulin remains unaltered after the formation of Au_{25}. The Au_{25} cluster was protected by insulin with noncovalent interactions and not through the Au−S bonds.[40] Theoretical studies have also shown that the interaction between gold clusters and amino acids is noncovalent in nature.[41,42] The immobilization of proteins using AuNCs and growth of these clusters within the protein may disrupt its secondary structural elements. Because the sequence dictates the structure of proteins and the structure of proteins determines their function, studies on the interaction of AuNCs with proteins are of high importance. Indeed, structural changes in the protein upon binding with the surface of the AuNCs through noncovalent interaction are not yet completely understood.

The biological function of proteins also depends on its internal dynamics in solution.[43] The changes in the secondary structure and internal motions of a protein thus lead to variations in its activity. Understanding such changes in structure and internal motions of proteins upon interaction with AuNCs is necessary for the application of these composites in nanotechnology.[44] Motivated by these facts, systematic docking studies and molecular dynamics simulation studies have been carried out in the present work to understand the interaction between lysozyme and Au_{25}. The internal motions have furthermore been assessed with the help of principal component analysis before and after the interaction with Au_{25}.

As mentioned above, gold clusters induce changes in the structure and dynamics of the lysozyme. Considering the relatively small dimension of the gold clusters, one can also expect changes in their structure, dynamics, and properties in the presence of lysozyme when compared to the clusters in an aqueous environment. There are detailed reports on such biomolecular induced changes of substrate molecules with implications on the imaging of the biostructures because often these are connected to changes in their absorption and fluorescence properties. These can be used as signatures to indicate the presence of specific biomolecules in a given sample.[45] To mention a few examples, in the presence of fibril-like biostructures, a red-shift in the absorption maximum and significant increase in fluorescence intensity is reported for thioflavin-T.[46] Similarly, in the presence of DNA-like biostructures, significant increase in the two-photon absorption cross section is reported for cyanine-like molecules.[47] It is notable that in the vicinity of a membrane-like environment, changes in absorption maximum and fluorescence intensity in prodan and its derivatives have been reported.[48] Keeping this in mind, we have also investigated the changes in the optical properties of the gold clusters using a damped linear response theory within a polarizable embedding scheme. We have thus studied the optical properties of a gold cluster in both water and lysozyme environments. The following important points have been addressed in this study:

(1) The changes in the secondary structure of lysozyme upon interaction with Au_{25}.
(2) The variation in the dynamical motions of lysozyme due to its interaction with Au_{25}.
(3) The changes in the optical properties of Au_{25} in the lysozyme environment.

COMPUTATIONAL DETAILS

The initial coordinates of lysozyme were taken from the protein data bank (PDB entry 2CDS), and coordinates for Au_{25} were downloaded from the Cambridge cluster database.[49] The structure of native lysozyme is shown in Figure S1 of the Supporting Information. It has α and β domains, where the α domain is made up of residues 1−35 and 85−129. In these sequence ranges, four α helices and a short 3_{10} helix are present. The β domain consists of a triple-standard antiparallel β sheet, a long loop, and a 3_{10} helix. These are found in the sequence starting from 36 to 84. The possible binding pockets for Au_{25} in lysozyme were identified through blind docking with the help of the patch dock software.[50,51] Results obtained from the above-mentioned protocol were refined with the help of the FireDock tool.[52,53] It can be seen from Figure 1 that the gold cluster can interact with the protein at four different binding sites. The most favorable docked structure was selected from each binding site. These protein−AuNC complexes are referred to as model-1, model-2, model-3, and model-4 in the remaining part of the text. The geometries of these complexes were used for further

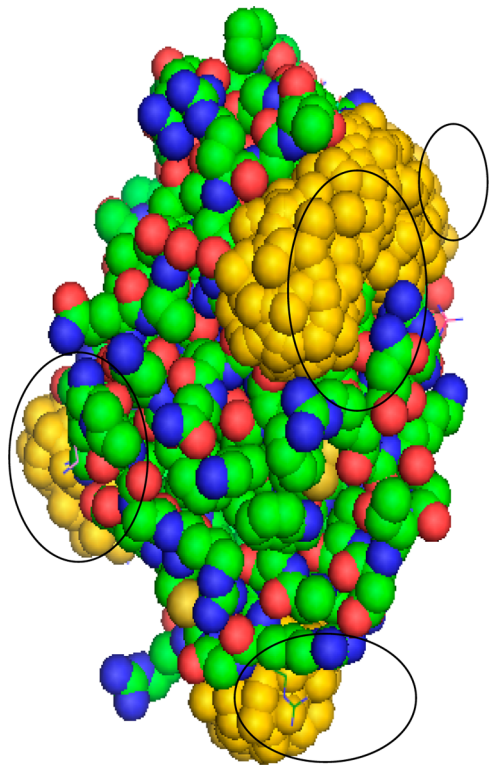

Figure 1. Superposition of docking results obtained from the FireDock algorithm. Circles indicate the most favorable binding sites.

dx.doi.org/10.1021/jp508582c | J. Phys. Chem. C XXXX, XXX, XXX−XXX

investigation using classical molecular dynamics (MD) and steered molecular dynamics (SMD) simulations.

The MD simulations were carried out for 50 ns using the GROMACS[54−56] (version 4.5.3.) package employing the AMBER99[57] force field for lysozyme. The force field parameters for the gold atoms were taken from a previous study.[58,24] Gold atoms were treated as Lennard-Jones particles with no charge. Each model was solvated with a TIP3P water molecules in a cubic box with cell length of roughly 71 Å. The overall positive charge on the lysozyme was neutralized by the inclusion of eight Cl^- ions. All models were subjected to energy minimization using the steepest decent method to relax the entire system. Temperature and pressure controls were imposed using the V-rescale and Parrinello−Rahman algorithms with a coupling constant of 0.1 ps and 2.0 ps, respectively.[59−61] MD simulations were carried out with a time step of 2 fs for 1 ns to equilibrate the models in the *NPT* ensemble. Using a time step of 2 fs, trajectories were collected over a 50 ns simulation and coordinates were saved every 0.2 ps. The electrostatic interactions were calculated using Particle Mesh Ewald with the interpolation order of 4 and a grid spacing of 1.6 Å.[62] Bonds between hydrogen and heavy atoms were constrained at equilibrium bond lengths using the LINCS algorithm.[63] The trajectories obtained from MD simulations were visualized with the help of the VMD package.[64] Further analysis of trajectories was performed with the tools available in the GROMACS package (version 4.5.3).[54−56]

The structures obtained from MD simulations were used for SMD simulation or center-of-mass pulling simulations. SMD simulations were carried out to pull away Au_{25} from the lysozyme−AuNC complex. A schematic representation of SMD simulation is shown in the Supporting Information (Figure S2). The same force field parameters were used for lysozyme, and also the same Lennard-Jones parameters were applied for Au_{25} to perform SMD simulations. All structures were solvated within a TIP3P water box. The equilibration was carried out for 1 ns in the *NPT* ensemble by restraining lysozyme and Au_{25}. During SMD simulations, lysozyme was fixed and Au_{25} was pulled away from the complex. The direction of the pulling was normal to the binding site in lysozyme. These simulations were carried out by restraining the position of lysozyme, and a trajectory was collected for 3 ns. A harmonic spring constant of 1000 kJ mol^{-1} nm^{-2} and pulling rate 0.001 nm ps^{-1} were used to pull the Au_{25}.

To investigate the biomacromolecule-induced structural effects on the optical properties of the AuNCs, we have investigated the optical properties of Au_{25} in both aqueous and lysozyme environments (in particular for the model-1) as well as in vacuum. The aim of the present investigation is to explore the differences in the one-photon absorption (OPA) spectra of the gold cluster when bound to lysozyme because this information can be used as a signature for probing proteins. To compute the OPA spectra for Au_{25}, we have optimized its geometry in isolation at the PBE0/LANL2DZ level.[65−70] For calculating the absorption spectra in the 500−800 nm spectral region, using time-dependent density functional theory (TD-DFT), it was necessary to include more than 60 excited states in the calculations, which made the OPA calculation very expensive and computationally demanding. For this reason, we decided to use a complex polarization propagator implementation within the TD-DFT approach.[71,72] For the calculations of the OPA properties of the gold cluster in the aqueous environment and in the protein milieu, we have used the recently developed polarizable embedding (PE) complex polarization propagator method.[73] A detailed derivation of both ground-state optimization and the coupling to response function expressions utilizing DFT can be found elsewhere, whether being conventional linear response theory[74,75] (nondamped) or damped linear response theory.[73] The PE method is an advanced QM/MM procedure in which, in general, the atoms defining the environment surrounding a region described using quantum mechanics (QM) is treated using a classical description in terms of localized multipoles and localized polarizabilities. The former mimics the permanent charge distribution of the environment, whereas the latter accounts for induction effects. However, in this study, we have restricted to the use of a point charge description of the environment. The expansion centers for the localized charges were taken at the atomic nuclei that define the environment (water or lysozyme). The optical properties of the Au_{25} cluster (the QM region) were calculated using the complex polarization propagator (CPP) method[76] coupled to PE for inclusion of environmental effects. In the PE-CPP approach, the absorption (here the ultraviolet spectrum) is calculated directly in terms of the imaginary part of the complex polarizability of the Au_{25} cluster. This has the advantage that, in contrast to conventional linear response theory, absorption because of higher-lying states may easily be calculated and that divergences in the underlying response equations are avoided. The PE-CPP approach, implemented in the developmental version of the Dalton program,[77] was used to calculate the absorption spectra of the Au_{25} cluster. All calculations utilize the CAM-B3LYP functional[78] and the Stuttgart effective core potential (SDD)[79] unless otherwise noted. As stated before, we have used a classical force field including only localized atomic charges to represent the environment, either water or protein. The charges were based on the force field used for carrying out MD simulations.

Analysis. In the following sections, short descriptions of the different analysis tools used to study the interaction between lysozyme and the Au_{25} cluster are provided.

Root Mean Square Deviation (RMSD). The RMSD, at time *t*, of the backbone atoms of the protein was calculated with reference to starting structure using the formula

$$\mathrm{RMSD}(t) = \left(\frac{1}{N} \sum_{i=1}^{N} \| r_i(t) - r_i(0) \|^2 \right)^{1/2} \quad (1)$$

The RMSD gives information about the deviation of the structure which is obtained from simulation, with reference to its initial structure.

Hydrogen Bonds. Hydrogen bonding interactions in lysozyme were calculated using

$$H_i = \begin{cases} 1, & d(H_i \cdots O_i) \leq 3.5 \text{ and} \\ & 120^\circ \leq \text{angle}(O_i \cdots H_i - N_i) \leq 180^\circ \\ 0, & \text{otherwise} \end{cases} \quad (2)$$

where H_i is an intramolecular hydrogen bond in the lysozyme, and the numbers of hydrogen bonds were calculated from the trajectory.

Secondary Structure Analysis. The secondary structure analysis of the protein was performed using the DSSP (dictionary of protein secondary structure: patterns recognition of hydrogen−bonded geometrical features) protocol available in the do_dssp module of the GROMACS package.[80] On the basis of hydrogen bonds and other geometrical parameters, this protocol can be used to determine the secondary structure of proteins.

dx.doi.org/10.1021/jp508582c | J. Phys. Chem. C XXXX, XXX, XXX−XXX

Principal Component Analysis (PCA). The PCA was carried out to identify concerted motions and also to analyze the inter-residue motions. It is based on the calculation of the covariance matrix using

$$C_{ij} = \langle (x_i - \langle x_i \rangle)(x_j - \langle x_j \rangle) \rangle \quad i, j = 1, 2, 3, \ldots 3N \qquad (3)$$

where x_i is the Cartesian coordinate of the ith backbone atom and N is the number of backbone atoms. A positive value of C_{ij} represents a correlation in motion between residues i and j and thus implies that the motions are in the same direction. A negative value of C_{ij} represents an anticorrelation motion between residues i and j, i.e., the atoms are moving in opposite directions. A value of zero represents that the atoms are moving independent of each other. The extent of correlation was obtained from the correlation coefficients as obtained from the covariance matrix.

RESULTS AND DISCUSSION

The docking poses as obtained from the FireDock tool are shown in Figure 2. It can be seen from this figure that in three models

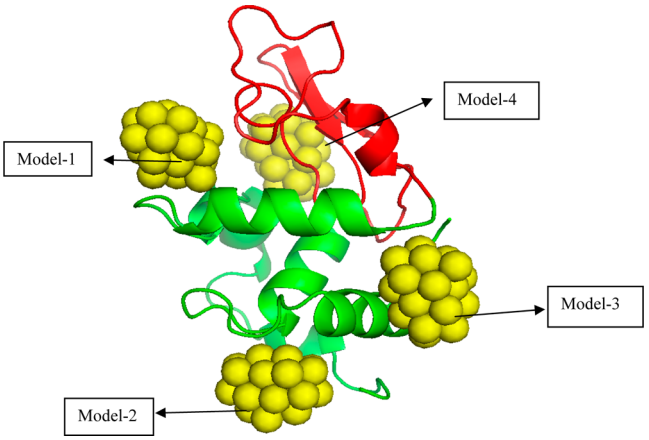

Figure 2. Favorable binding sites for Au_{25}. Green, α domain; red, β domain.

(model-1, model-2, and model-3), Au_{25} interacts with the α domain. In model-4, Au_{25} binds with both α and β domains. The former domain of lysozyme contains a core of side chains of hydrophobic amino acids that are packed closely together. The residues, which are in contact with Au_{25} within 5 Å in all the models, are shown in Table 1. It can be seen from the results that both Glu35 and Asp52 in the active site of lysozyme interact with Au_{25} in model-4. In all other models, arginine (Arg14, Arg21, Arg45, Arg73, Arg112, and Arg128), aspartic acid (Asp18, Asp48, Asp52, Asp87, and Asp101), asparagine (Asn19, Asn44, Asn59, Asn103, and Asn106), and alanine (Ala9, Ala10, Ala11, Ala107, and Ala110) residues participate in the interaction with Au_{25}. Further, both tryptophan (Trp62 and Trp63) and tyrosine (Tyr20 and Tyr23) stack on the surface of Au_{25}. Both histidine and cysteine interact with Au_{25} in model-2 and model-3.

To understand the stability of lysozyme-Au_{25} complexes (model-1 to model-4), MD simulations were carried out for 50 ns using the AMBER99 force field. Visual inspection of the trajectories obtained from MD simulation show that the interaction of Au_{25} and protein is stable throughout the 50 ns. Au_{25} is stabilized by both hydrophobic and hydrophilic interaction of the residues in all the models. Various amino acids that interact with Au_{25} before and during MD simulation are given in Table 1. During MD simulation, other amino acids such as Trp108, Val109, Cys6, and Lys13 participate in the interaction with Au_{25}. The structural deviations in lysozyme were calculated with the help of the RMSD with reference to the initial structure. The changes in RMSD values with time for the various models are given in Figure 3. The average RMSD value for native lysozyme and models-1, -2, -3, and -4 are 1.65, 0.80, 0.84, 1.72, and 1.27 Å, respectively. It can be seen from Figure 3 that model-1 and model-2 are more stable than native lysozyme. In the case of model-3, RMSD values of lysozyme are higher than those of the native lysozyme. Model-3 has the highest RMSD value among all the models. Further, these RMSD values of all the models show that the systems are well-equilibrated.

SMD simulations were used to compare the binding affinity of the different models based on the hypothesis that "a larger force is needed to unbind a ligand from the binding site with higher affinity". The force required to unbind Au_{25} is given in Figure 4. From the results it can be clearly seen that the unbinding of Au_{25} from the binding site of lysozyme in model-3 requires a force that is greater than that required in other models. The time taken to pull the cluster varies as model-3 > model-4 > model-2 > model-1. The residues that possess strong interaction with Au_{25} during the SMD simulation for each model were obtained, and the results are presented in Table 2. It can be noted that the higher binding affinity of model-3 is due to the interaction of Au_{25} atoms with a greater number of residues from lysozyme via nitrogen, oxygen, and sulfur atoms.

Previous studies have revealed that nanomaterials such as carbon nanotubes and graphene perturb the secondary structure of peptides and proteins.[81−83] The changes in the hydrogen bonding pattern after interaction with Au_{25} are derived from the MD trajectories. The number of hydrogen bonds present in the lysozyme during the MD simulation is depicted in Figure S3 of the Supporting Information. The average number of hydrogen bonds for native lysozyme and models-1, -2, -3, and -4 is 56, 54, 56, 51, and 53, respectively. The number of hydrogen bonds in model-2 fluctuates around its average value throughout the simulation, while in models-1, -3, and -4, the number of hydrogen bonds decreases during the simulation. Results obtained from the DSSP analysis are plotted in Figure S4 of the Supporting Information. The result illustrates the residue-wise conformational changes upon interaction with Au_{25}. Interestingly, there is not much change in the secondary structural elements in models-1, -2, and -4 in contrast to the native lysozyme. It can be noted from the results of model-3 that there are significant changes in the secondary structure when compared to that of the native lysozyme. The small 3_{10} helix (Met105, Ala106, and Asn107) of lysozyme in model-3 changes to turn upon interaction with Au_{25}. The α helices ((Ala110, Arg112, Trp113, Asn113, Arg114, and Cys115), (Ala32, Lys33, Phe34, and Glu35)) of lysozyme undergo conformational changes to turns because of its interaction with Au_{25}. Residues present near the interaction site undergo appreciable conformational variations. These findings are in accordance with the results obtained from the hydrogen bond analysis. In model-3, conformational alterations are not observed at the binding site of Au_{25}. The variations in the number of contacts between the residues of lysozyme and Au_{25} were analyzed using trajectory as obtained from MD simulation. As evident from Figure S5 of the Supporting Information, there is a significant increase in the number of contacts between Au_{25} and lysozyme in model-3, wherease there are no appreciable changes in the other models. The higher number of contacts in model-3 induces the conformational changes by affecting the fraction of

dx.doi.org/10.1021/jp508582c | J. Phys. Chem. C XXXX, XXX, XXX−XXX

Table 1. Amino Acids of Lysozyme Which Are in Contact with Au_{25}

from docking				during simulation			
model-1	model-2	model-3	model-4	model-1	model-2	model-3	model-4
Asn59	Lys1	Ala9	Phe34	Arg58	Lys1	Cys6	Phe34
Trp62	Glu7	Ala10	Glu35	Asn59	Phe3	Ala10	Ser36
Trp63	Ala10	Lys13	Asn44	Trp62	Cys6	Met12	Asn44
Arg73	Ala11	Asp18	Arg45	Arg73	Glu7	Lys13	Arg45
Leu75	Arg14	Asn19	Thr47	Leu75	Leu8	Leu17	Asn46
Lys97	His15	Tyr20	Asp48	Lys97	Ala10	Asp18	Thr47
Ile98	Thr40	Arg21	Asp52	Ile98	Ala11	Asn19	Asp48
Asp101	Ser86	Tyr23	Gln57	Asp101	Met12	Tyr20	Gly49
Gly102	Asp87	Ser24	Asn59	Gly102	Lys13	Arg21	Ser50
Asn103	Ile88	Leu25	Gln70	Asn103	Arg14	Gly22	Thr51
Asn106	Thr89	Gly26	Val109	Gly104	His15	Tyr23	Asp52
Ala107	Val92	Gln121	Ala110	Asn106	Thr40	Ser24	Leu56
Arg112		Ile124		Ala107	Ser85	Leu25	Gln57
		Cys127		Trp108	Ser86	GLY26	Asn59
		Arg128		Val109	Asp87	Asn27	Ala107
		Leu129		Arg112	Ile88	Val29	Trp108
					Thr89	Val120	Val109
					Val92	Gln121	Ala110
					Arg128	Ile124	Trp111
					Leu129	Arg125	Arg112
						Cys127	Asn113
						Arg128	
						Leu129	

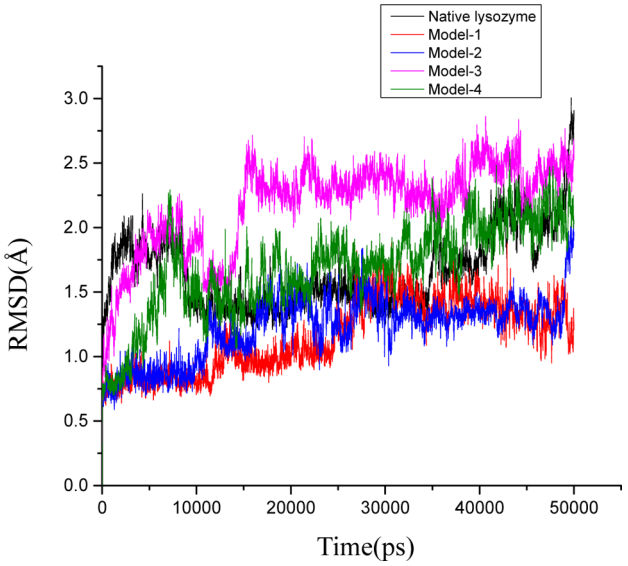

Figure 3. Root-mean-square deviation (RMSD) for all models.

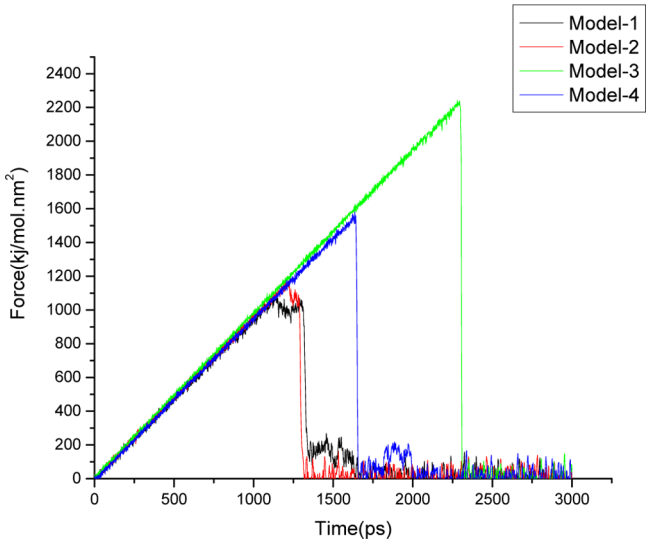

Figure 4. Calculated potential of mean force (PMF) for all models as obtained from steered molecular dynamics simulations.

hydrogen bonds. Pradeep and co-workers reported that the loss in helical content of lysozyme during the formation of Au_{10} or Au_{12} is due to the breakage of disulfide bonds.[38] Therefore, in addition to breaking of disulfide bonds, the changes in the noncovalent interactions also induce conformational alterations in lysozyme. The Au_{10} or Au_{12} cluster is present inside one lysozyme and not sourrounded by several lysozyme molecules. Similar to the native lysozyme, the lysozyme with Au_{10} or Au_{12} also forms the aggregates such as dimer, trimer, and tetramer. The Au_{10} or Au_{12} clusters present in the dimer, trimer, and tetramer are not forming the aggregates of Au_{20} or Au_{24}. In the present study, the Au_{25} cluster is present on the surface of the lysozyme. This cluster can be surrounded by the other lysozyme molecules, and it can form the aggregates of Au_{25}. It can be seen from Table 1 and Table 2 that Au_{25} have interaction with cystiene in model-2 and model-3. However, only in model-3 is the strong interaction between cystiene and Au_{25} found. The covalent binding of gold to the cysteine is experimentally known in the protein immobilization. It adds to the enormous computational difficulties when one wants to model the interface region in the metal nanocluster chemically bound to biological macromolecules. The simplistic approach is to employ a noncovalent interaction between these two subsystems, and this still provides valuable information about the AuNC-induced secondary structural changes in lysozyme in model-3.

dx.doi.org/10.1021/jp508582c | J. Phys. Chem. C XXXX, XXX, XXX−XXX

Table 2. Residues Possessing Strong Interaction with Au_{25} in All the Lysozyme−Au_{25} Models

model-1	model-2	model-3	model-4
Arg73 (N)	Lys1 (N)	Arg 21 (N)	Arg45 (N)
Asp101 (O)	Phe3 (C)	Lys13 (N)	Asn44 (N)
Gly102 (N)	Glu7 (O)	Asn19 (N)	Asn46 (N)
Asn103 (H)	Ser 86 (H)	Cys127 (S)	Thr47 (N)
Trp62 (C)	Ala10 (H)	Tyr 20 (OH)	Asp52 (O)
	Arg14 (N)	Arg125 (H)	Glu35 (O)
	His15 (N)	Asp18 (O)	Ser36 (N)
	Asp87 (O)	Ser24 (O)	Ala110 (H)
		Leu25 (N)	
		Gly26 (N)	

The PCA analysis was used to extract collective motions, which are related to the protein function, using the eigenvectors of the covariance matrix and thus the conformational space of the molecule. The PCA analysis was performed using the g_covar and g_anaeig programs implemented in the GROMACS suite. Both rotational and translational motions were removed by fitting the backbone atoms of lysozyme of each frame to the starting conformation. Eigenvalues and eigenvectors were calculated by diagonalizing the covariance matrix. The covariance matrix shows the nature of the inter-residue motions of lysozyme. The results are plotted in Figure 5. Blue indicates anticorrelated motion, and red represents correlated motion between the residues of lysozyme. It can be seen from Figure 5 that the native lysozyme has more anticorrelated motions between the residues. Model-2 and model-3 exhibit enhanced correlated and anticorrelated motions. The anticorrelated motions between the residues of lysozyme in the models (model-1 and model-4) are marginal compared to that of native lysozyme. The eigenvectors give the directions of motion, and the eigenvalues represent the amount of variations along the eigenvectors. Figure S6 of the Supporting Information demonstrates the variance in the conformational space covered by the first 20 principal components of lysozyme for all the models. It can be seen from this figure that the top 10 principal components account for 40%, 52%, 48%, 40%, and 16% of variations for the native lysozyme, model-1, model-2, model-3, and model-4, respectively. The 10 largest eigenvalues (principal components) corresponding to the first 10 eigenvectors and their cumulative percentages are presented in Table 3. The associated eigenvalue of each eigenvector gives the total mobility of the protein. It can be seen from the table that the total cumulative percentage is the same for native lysozyme and model-3, but their eigenvalues are different. The variation of the first eigenvector in model-4 is the minimum, whereas in model-2 it is the maximum. The values of the remaining principal components (EV2 to EV10) in model-1 and model-2 are different than those of the native lysozyme and the other models. The eigenvalue profile of models (model-1, model-2, model-3, and model-4) significantly deviates from the native lysozyme upon interaction with Au_{25}. It was observed in previous studies that the activity of mutated lysozyme is different from the native lysozyme,[84−86] and this was attributed to the changes in the eigenvalues of the mutated lysozyme compared to that of the native lysozyme.[87] The projection of the first five eigenvectors onto the root-mean-square-fluctuations (RMSF) of the residues as obtained from the MD trajectory was performed to calculate the magnitude of fluctuations of residues in the first five eigenvectors for all the systems. The results are plotted in Figure 6. The residue-wise fluctuations extracted from the first five eigenvectors are different in all the systems. The magnitude of the fluctuation of residues of lysozyme in model-1 to model-4 is enhanced compared to that of the native lysozyme. Except for the terminal residues, the RMSF of lysozyme corresponding to each eigenvector shows that the highest fluctuation is found in model-3. The catalytic active site residues of lysozyme are Asp52 and Glu35. The residues clustered around the catalytic residues are Asp101, Trp62, Trp63, Trp57, Phe3, Gly4, Gly16, Gly22, Ser24, Cys30, Ser36, and Gly117.[88] The RMSF of these residues in the first five eigenvectors of the systems model-1, model-2, model-3, and model-4 are also increased compared to that of lysozyme. Many studies have shown the importance of internal motions of residues near catalytic active site in the biological function of lysozyme.[89−91] ^{15}N NMR relaxation measurements have revealed that the biological activity of lysozyme is related to the mobility of residues present in the active site region.[89] The deletion of both Arg14 and His15 in lysozyme has enhanced its activity toward glycol chitin when compared to that of wild-type lysozyme because of the enhancement in the internal motions of the residues in the active site region.[91] In accordance with the previous seminal findings, the changes in the internal motion of lysozyme upon interaction with Au_{25} may enhance the activity of the lysozyme.[89,91]

Often, a strong correlation between the structure of a metal cluster and its optical properties is found. With an increase in the number of atoms, the cluster size usually increases and the absorption spectra of smaller-sized particles is blue-shifted because of the quantum confinement effect. Furthermore, with the increase in the cluster size, the number of local minima is also increased substantially. In the case in which different structures are not separated by large kinetic barriers, the properties can have contributions from all the conformations. Finite temperature simulations can account for the sampling over different structures of the atomic clusters that can contribute to the optical properties, which in fact has been one of the objectives of the current study. The Au_{25} itself can exist in different symmetries, and in particular we considered here clusters with C_{2v} and D_{2h} symmetries. The energetics of the geometry-optimized clusters suggest that the cluster with C_{2v} symmetry is the most stable one. It is worth mentioning that this also corresponds to the minimum as predicted from the Sutton−Chen potential. Absorption spectra for thiolated and other ligated Au_{25} gold clusters are reported experimentally. Unfortunately there are no experimental or previous theoretical results on the absorption spectra of this gold cluster when it is bound to lysozyme. Below, we will briefly review and discuss available data on absorption spectra of gold clusters (Au_{25} and other small clusters) with different ligands,[92−100] and with that background we will discuss our results.

There are different views in the literature on the ligation effect on the optical properties of AuNCs. There are reports that suggest substantial changes in the absorption and fluorescence properties of gold clusters due to ligation.[92] Other studies show contrary results.[93−100] In other words, except for the shift in the absorption wavelength and corresponding intensities, the overall spectral pattern is conserved for a specific gold cluster.[93−100] However, the fluorescence properties have been reported to be dependent on the ligating group. It is worth mentioning that the former study was limited to small clusters (such as Au_2−Au_4)[92] while the latter correspond to bigger clusters like Au_{25}.[93−100] It is quite natural that when the cluster size is small, one can expect its electronic structure and geometry to be significantly altered by the changes in the environment or because of ligation. The

dx.doi.org/10.1021/jp508582c | J. Phys. Chem. C XXXX, XXX, XXX−XXX

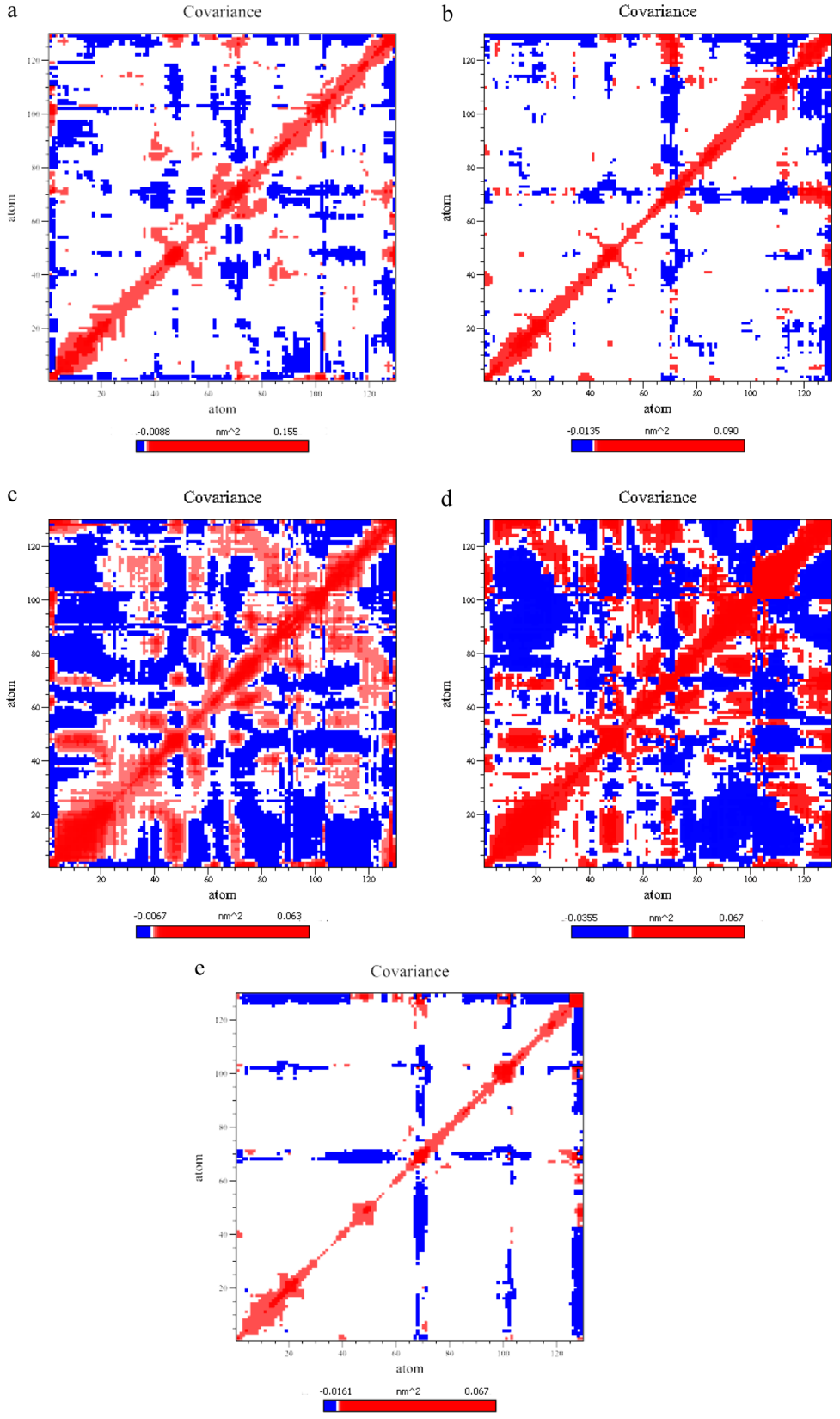

Figure 5. Covariation of motion for (a) native lysozyme, (b) model-1, (c) model-2, (d) model-3, and (e) model-4.

changes in the structure may not be significant for larger clusters, and one can expect only environment- or ligand-induced changes in the electronic structure of these clusters. As we mentioned previously, only changes in the peak positions and corresponding intensities are observed. We note that the peaks appearing at 650 (peak 1), 450 (peak 2), and 400 (peak 3) nm are seen in all Au_{25} clusters independent of the ligating agents or environment.[93−100] Both peak 1 and peak 2 are known to shift position specific to

dx.doi.org/10.1021/jp508582c | J. Phys. Chem. C XXXX, XXX, XXX−XXX

Table 3. Eigenvalues of the First Five Eigenvectors of all Model Complexes[a]

models	EV1	EV2	EV3	EV4	EV5	EV6	EV7	EV8	EV9	EV10	cumulative percentage
NL	13.726	11.089	4.265	2.811	1.877	1.642	1.544	1.019	0.809	0.775	40
model-1	15.046	9.811	7.332	4.330	3.575	3.178	2.994	2.231	2.025	1.810	52
model-2	17.454	6.842	5.056	4.366	3.760	3.168	2.288	2.021	1.734	1.600	48
model-3	16.377	8.271	5.092	3.056	1.860	1.432	1.223	1.028	0.893	0.703	40
model-4	8.956	1.931	1.159	1.059	0.803	0.694	0.505	0.470	0.389	0.352	16

[a]NL, native lysozyme; EV, eigenvalue.

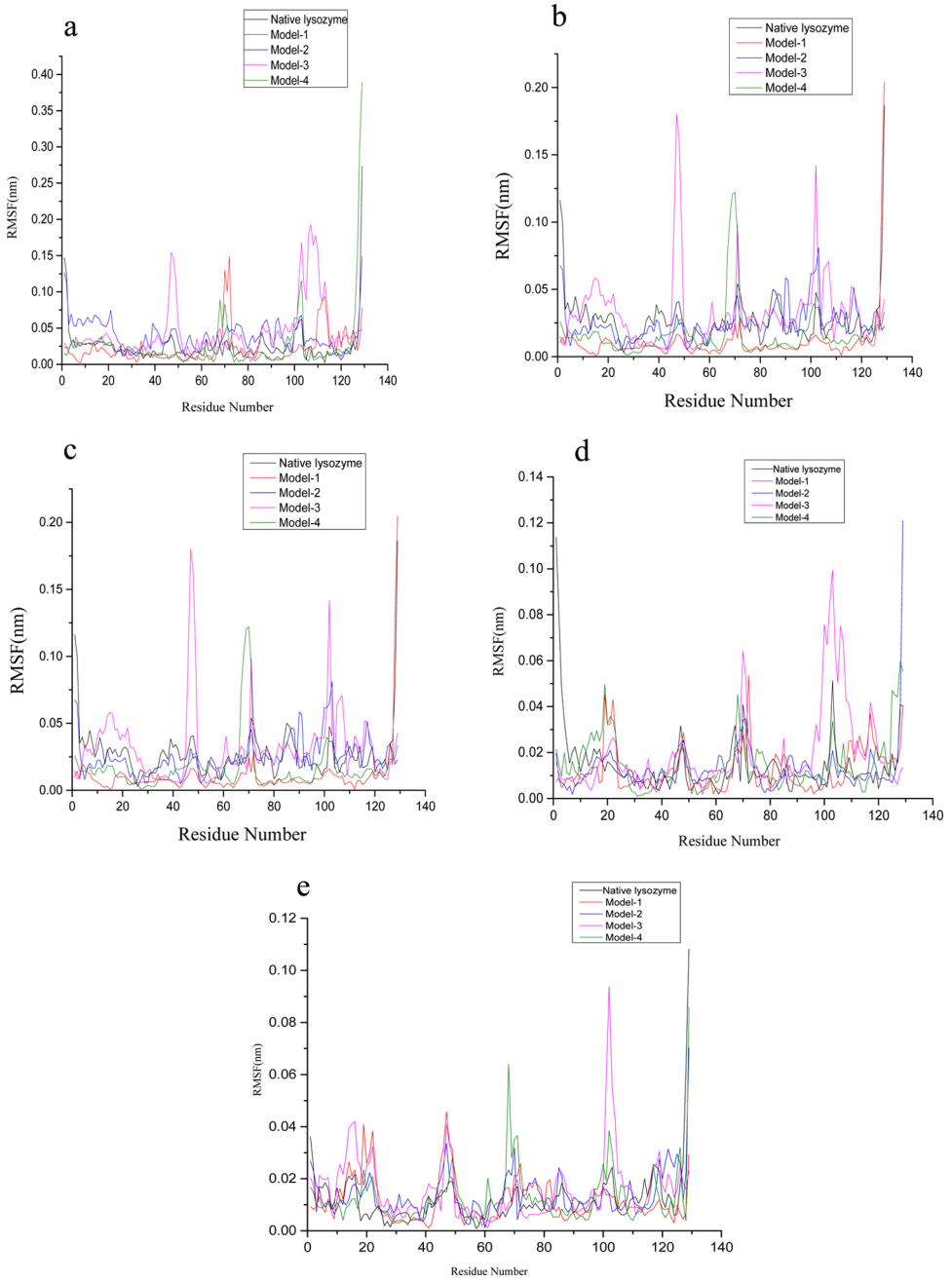

Figure 6. Root-mean-square fluctuation of residues extracted from first five eigenvectors: (a) eigenvector1, (b) eigenvector2, (c) eigenvector3, (d) eigenvector4, and (e) eigenvector5.

different ligation. In particular, when the ligand group changed from glutathione (GSH) to 3-mercaptopropyl)trisilanol (MPS), peak 1 showed a red shift by 10 nm.[93,96] Similarly, changing the ligation from $Se(C_2H_4Ph)$ to $S(C_2H_4Ph)$ in nanoclusters $Au_{25}(SeC_2H_4Ph)_{18}$ yielded red shifts of 8 and 20 nm in the first and second peaks, respectively.[97,98] Furthermore, a comparison of the spectra of $Au_{25}(SeC_2H_4Ph)_{18}$ and $Au_{25}(SePh)_{18}$ showed a red shift by 30−50 nm in all three peaks, which suggests that the effect is due to the fact that the additional conjugation in the ligand yields stronger shifts than the

dx.doi.org/10.1021/jp508582c | J. Phys. Chem. C XXXX, XXX, XXX−XXX

substitution of S by Se.[97,98] These experimental reports clearly suggest that the peak positions are sensitive to ligation and also to the dielectric nature of the microenvironment. The motivation of the current work is to seek any lysozyme-induced change in the optical properties of AuNC which can be further used as a "colorimetric signature" to sense or detect lysozyme, and for this reason the absorption spectra for only Au_{25} has been computed in water and in lysozyme environments.

The one-photon absorption spectra computed for Au_{25} in aqueous and lysozyme environments are shown in Figures S7 and S8 of the Supporting Information, respectively. The average absorption spectra of Au_{25} in water and lysozyme alone when compared to the one calculated based on the optimized geometry of Au_{25} in vacuum are shown in Figure 7. Only the absorption

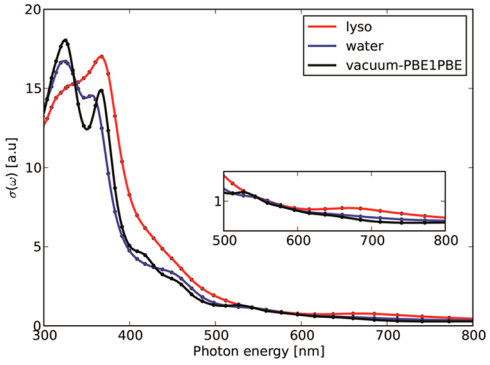

Figure 7. Averaged absorption spectrum of Au_{25} in vacuum, water environment, and protein environment.

wavelength range from 300 to 800 nm is shown, which corresponds to the visible region of the spectrum. As can be seen, all the features observed in the case of thiolated gold cluster are also seen in this spectrum. For example, peak 1 appears between 600 and 800 nm and the shoulder appearing around 400−500 refers to peak 2 and the peak 3 appears around 375 nm. The first peak having an absorption maximum at 700 nm gains intensity, as has been reported in the case of thiolated cluster. It can be seen from Figure 7 that the peak positions are shifted when going from water-like to lysozyme environment. Because the spectra correspond to finite temperature structures at room temperature, the peak positions are broadened, making it difficult to calculate the exact shift in each of the three peaks. However, it is clearly established that peak 2 and peak 3 are red-shifted in the lysozyme-like environment when compared to those in water, which further can be used for colorimetric sensing of lysozyme. A similar red shift in the peak positions has been reported during the phase-transfer reaction of Au_{25} cluster from water to toluene-like medium.[99] It is possible to attribute the red shift in Au_{25} spectra to the change from a hydrophilic-like to a hydrophobic-like environment. The lysozyme environment-dependent features observed in the case of the gold cluster can clearly be used as signatures for sensing lysozyme and similar biomolecules.

CONCLUSION

The interaction of Au_{25} with lysozyme has been studied using molecular docking and molecular dynamics simulations. It has been shown that Au_{25} can interact at different sites of lysozyme. The interaction is stabilized by the binding of gold nanoclusterss with both hydrophilic and hydrophobic amino acids. The secondary structural changes of lysozyme upon interaction with Au_{25} depend on the interacting site. The strong binding of Au_{25} induces the structural changes in the helices of lysozyme. The variations in the internal motions of the lysozyme also depend on the site-specific interaction. The correlated and uncorrelated motions of residues in lysozyme increase upon interaction with Au_{25}. The binding of Au_{25} alters the inter-residue motions and increases the magnitude of fluctuation. The motions of the residues in the active site region are also enhanced. The interaction of Au_{25} with lysozyme brings changes in its secondary structure and internal motions, which are important for its function. Therefore, Au_{25} can change the biological function of the protein, and it may increase or decrease the activity of the protein. Overall, the results demonstrate that the functionality of lysozyme-like biomaterials can be modulated by AuNCs. Furthermore, this study reports characteristic lysozyme-dependent features in the absorption spectra of gold nanoclusters that can be exploited for the use of gold nanocluster imaging and sensing applications of lysozyme-like biomolecules.

ASSOCIATED CONTENT

Supporting Information

Structure of native lysozyme (Figure S1); schematic showing steered molecular dynamics of the lysozyme−Au_{25} complexes (Figure S2); number of hydrogen bonds in the native lysozyme and lysozyme−Au_{25} complexes as obtained from the 50 ns MD simulation (Figure S3); variations in the secondary structure of lysozyme in all model complexes (Figure S4); number of contacts between Au_{25} and the residues of lysozyme in all models during the MD simulation (Figure S5); variance in the conformational space covered by the first 20 principal components of native lysozyme, model-1, model-2, model-3, and model-4 (Figure S6); absorption spectra of Au_{25} embedded in water (Figure S7) and in lysozyme (Figure S8). This material is available free of charge via the Internet at http://pubs.acs.org.

AUTHOR INFORMATION

Corresponding Author

*Tel.: +91 44 24411630. Fax: +91 44 24911589. E-mail: subuchem@hotmail.com, subbu@clri.res.in.

Notes

The authors declare no competing financial interest.

ACKNOWLEDGMENTS

We thank the Board of Research in Nuclear sciences (BRNS), Mumbai, India, and Nanomaterial−Safety, Health and Environment (NanoSHE BSC0112) project funded by Council of Scientific and Industrial Research (CSIR) New Delhi, India, for Financial Support. S.K.M. thanks Department of Science and Technology (DST), New Delhi, India for providing INSPIRE Fellowship (Inspire Fellow). J.K. thanks The Danish Councils for Independent Research for financial support. This work was also supported by a grant from the Swedish Infrastructure Committee (SNIC) for the project "Multiphysics Modeling of Molecular Materials", SNIC 023/07-18.

REFERENCES

(1) Bigioni, T. P.; Whetten, R. L.; Dag, O. Near-Infrared Luminescence from Small Gold Nanocrystals. *J. Phys. Chem. B* **2000**, *104*, 6983−6986.

(2) Huang, T.; Murray, R. W. Visible Luminescence of Water-Soluble Monolayer-Protected Gold Clusters. *J. Phys. Chem. B* **2001**, *105*, 12498−12502.

(3) Link, S.; Beeby, A.; FitzGerald, S.; El-Sayed, M. A.; Schaaff, T. G.; Whetten, R. L. Visible to Infrared Luminescence from a 28-Atom Gold Cluster. *J. Phys. Chem. B* **2002**, *106*, 3410−3415.

(4) Yang, Y.; Chen, S. Surface Manipulation of the Electronic Energy of Subnanometer-Sized Gold Clusters: An Electrochemical and Spectroscopic Investigation. *Nano Lett.* **2003**, *3*, 75−79.
(5) Zheng, J.; Petty, J. T.; Dickson, R. M. High Quantum Yield Blue Emission from Water-Soluble Au_8 Nanodots. *J. Am. Chem. Soc.* **2003**, *125*, 7780−7781.
(6) Negishi, Y.; Takasugi, Y.; Sato, S.; Yao, H.; Kimura, K.; Tsukuda, T. Magic-Numbered Au_n Clusters Protected by Glutathione Monolayers (n = 18, 21, 25, 28, 32, 39): Isolation and Spectroscopic Characterization. *J. Am. Chem. Soc.* **2004**, *126*, 6518−6519.
(7) Chen, S.; Ingram, R. S.; Hostetler, M. J.; Pietron, J. J.; Murray, R. W.; Schaaff, T. G.; Khoury, J. T.; Alvarez, M. M.; Whetten, R. L. Gold Nanoelectrodes of Varied Size: Transition to Molecule-like Charging. *Science* **1998**, *280*, 2098−2101.
(8) Hicks, J. F.; Templeton, A. C.; Chen, S. W.; Sheran, K. M.; Jasti, R.; Murray, R. W.; Debord, J.; Schaaf, T. G.; Whetten, R. L. The Monolayer Thickness Dependence of Quantized Double-Layer Capacitances of Monolayer-Protected Gold Clusters. *Anal. Chem.* **1999**, *71*, 3703−3711.
(9) Hicks, J. F.; Miles, D. T.; Murray, R. W. Quantized Double-Layer Charging of Highly Monodisperse Metal Nanoparticles. *J. Am. Chem. Soc.* **2002**, *124*, 13322−13328.
(10) Quinn, B. M.; Liljeroth, P.; Ruiz, V.; Laaksonen, T.; Kontturi, K. Electrochemical Resolution of 15 Oxidation States for Monolayer-Protected Gold Nanoparticles. *J. Am. Chem. Soc.* **2003**, *125*, 6644−6645.
(11) Zhu, Y.; Qian, H.; Drake, B. A.; Jin, R. Atomically Precise $Au_{25}(SR)_{18}$ Nanoparticles as Catalysts for the Selective Hydrogenation of α,β-Unsaturated Ketones and Aldehydes. *Angew. Chem., Int. Ed.* **2010**, *49*, 1295−1298.
(12) Palmal, S.; Jana, N. R. Gold Nanoclusters with Enhanced Tunable Fuorescence as Bioimaging Probes. *Wiley Interdiscip. Rev.: Nanomed. Nanobiotechnol.* **2014**, *6*, 102−110.
(13) Xavier, P. L.; Chaudhari, K.; Baksi, A.; Pradeep, T. Protein-Protected Luminescent Noble Metal Quantum Clusters: An Emerging Trend in Atomic Cluster Nanoscience. *Nano Rev.* **2012**, *3*, 14767.
(14) Zheng, J.; Nicovich, P. R.; Dickson, R. M. Highly Fluorescent Noble-Metal Quantum Dots. *Annu. Rev. Phys. Chem.* **2007**, *58*, 407−431.
(15) Zheng, J.; Zhang, C. W.; Dickson, R. M. Highly Fluorescent, Water-Soluble, Size-Tunable Gold Quantum Dots. *Phys. Rev. Lett.* **2004**, *93*, 077402.
(16) Jin, R. Quantum Sized, Thiolate-Protected Gold Nanoclusters. *Nanoscale* **2010**, *2*, 343−362.
(17) Lin, C. A. J.; Lee, C. H.; Hsieh, J. T.; Wang, H. H.; Li, J. K.; Shen, J. L.; Chan, W. H.; Yeh, H. I.; Chang, W. H. Synthesis of Fluorescent Metallic Nanoclusters Toward Biomedical Application: Recent Progress and Present Challenges. *J. Med. Biol. Eng.* **2009**, *29*, 276−283.
(18) Shang, L.; Dong, S. J.; Nienhaus, G. U. Ultra-Small Fluorescent Metal Nanoclusters: Synthesis and Biological Applications. *Nano Today* **2011**, *6*, 401−418.
(19) Zheng, J.; Zhou, C.; Yu, M.; Liu, J. Different Sized Luminescent Gold Nanoparticles. *Nanoscale* **2012**, *4*, 4073−4083.
(20) Elghanian, R.; Storhoff, J. J.; Mucic, R. C.; Letsinger, R. L.; Mirkin, C. A. Selective Colorimetric Detection of Polynucleotides Based on the Distance-Dependent Optical Properties of Gold Nanoparticles. *Science* **1997**, *277*, 1078−1081.
(21) Alivisatos, A. P.; Johnsson, K. P.; Peng, X. G.; Wilson, T. E.; Loweth, C. J.; Bruchez, M. P.; Schultz, P. G. Organization of Nanocrystal Molecules Using DNA. *Nature (London, U.K.)* **1996**, *382*, 609−611.
(22) Mirkin, C. A.; Lestinger, R. L.; Mucic, R. C.; Storhoff, J. J. A DNA-Based Method for Rationally Assembling Nanoparticles into Macroscopic Materials. *Nature (London, U.K.)* **1996**, *382*, 607−609.
(23) Lee, O. S.; Schatz, G. C. Molecular Dynamics Simulation of DNA-Functionalized Gold Nanoparticles. *J. Phys. Chem. C* **2009**, *113*, 2316−2321.
(24) Lee, O. S.; Schatz, G. C. Interaction between DNAs on a Gold Surface. *J. Phys. Chem. C* **2009**, *113*, 15941−15947.
(25) Palmer, R. E.; Leung, C. Immobilization of Proteins by Atomic Clusters on Surfaces. *Trends in Biotechnol.* **2007**, *25*, 48−55.
(26) Prisco, U.; Leung, C.; Xirouchaki, C.; Jones, C. H.; Heath, J. K.; Palmer, R. E. Residue-Specific Immobilization of Protein Molecules by Size-Selected Clusters. *J. R. Soc., Interface* **2005**, *2*, 169−175.
(27) Purusottam, J.; Welford, C. A. Chapter 14 − Interfacing Cluster Physics with Biology at the Nanoscale. In *Nanoclusters: A Bridge Across Disciplines*; Elsevier: Amsterdam, 2010; Vol. *1*.
(28) Ackerson, C. J.; Powell, R. D.; Hainfeld, J. F. Site-Specific Biomolecule Labeling with Gold Clusters. *Methods Enzymol.* **2010**, *481*, 195−230.
(29) Retnakumari, A.; Setua, S.; Menon, D.; Ravindran, P.; Muhammed, H.; Pradeep, T.; et al. Molecular Receptor Specific, Non-Toxic, Near-Infrared Emitting Au Cluster-Protein Nanoconjugates for Targeted Cancer Imaging. *Nanotechnology* **2010**, *21*, 055103.
(30) Xavier, P. L.; Chaudhari, K.; Verma, P. K.; Pal, S. K.; Pradeep, T. Luminescent Quantum Clusters of Gold in Transferrin Family Protein, Lactoferrin Exhibiting FRET. *Nanoscale* **2010**, *2*, 2769−2776.
(31) Yan, L.; Cai, Y.; Zheng, B.; Yuan, H.; Guo, Y.; Xiao, D.; et al. Microwave-Assisted Synthesis of BSA-Stabilized and HSA Protected Gold Nanoclusters with Red Emission. *J. Mater. Chem.* **2012**, *22*, 1000−1005.
(32) Chaudhari, K.; Xavier, P. L.; Pradeep, T. Understanding the Evolution of Luminescent Gold Quantum Clusters in Protein Templates. *ACS Nano* **2011**, *5*, 8816−8827.
(33) Lin, Y. H.; Tseng, W. L. Ultrasensitive Sensing of Hg^{2+} and CH_3Hg Based on The Fluorescence Quenching of Lysozyme Type VI-Stabilized Gold Nanoclusters. *Anal. Chem.* **2010**, *82*, 9194−9200.
(34) Wen, F.; Dong, Y.; Feng, L.; Wang, S.; Zhang, S.; Zhang, X. Horseradish Peroxidase Functionalized Fluorescent Gold Nanoclusters for Hydrogen Peroxide Sensing. *Anal. Chem.* **2011**, *83*, 1193−1196.
(35) Wei, H.; Wang, Z.; Yang, L.; Tian, S.; Hou, C.; Lu, Y. Lysozyme Stabilized Gold Fluorescent Cluster: Synthesis and Application as Hg^{2+} Sensor. *Analyst (Cambridge, U.K.)* **2010**, *135*, 1406−1410.
(36) Lystvet, S. M.; Volden, S.; Singh, G.; Yasuda, M.; Halskau, O.; Glomm, W. R. Tunable Photophysical Properties, Conformation and Function of Nanosized Protein-Gold Constructs. *RSC Adv.* **2013**, *2*, 482−495.
(37) Chen, W. Y.; Lin, J. Y.; Chen, W. J.; Luo, L.; Diau, E. W. G.; Chen, Y. C. Functional Gold Nanoclusters as Antimicrobial Agents for Antibioticresistant Bacteria. *Nanomedicine* **2010**, *5*, 755−764.
(38) Ananya, B.; Paulrajpillai, L. X.; Kamalesh, C.; Goswami, N.; Palc, S. K.; Pradeep, T. Protein-Encapsulated Gold Cluster Aggregates: The Case of Lysozyme. *Nanoscale* **2013**, *5*, 2009−2016.
(39) Xie, J.; Zheng, Y.; Ying, J. Y. Protein-Directed Synthesis of Highly Fluorescent Gold Nanoclusters. *J. Am. Chem. Soc.* **2009**, *131*, 888−889.
(40) Liu, C. L.; Wu, H. T.; Hsiao, Y. H.; Lai, C. W.; Shih, C. W.; Peng, Y. K.; Tang, K. C.; Chang, H. W.; Chien, Y. C.; Hsiao, J. K.; Cheng, J. T.; Chou, P. T. Insulin-Directed Synthesis of Fluorescent Gold Nanoclusters: Preservation of Insulin Bioactivity and Versatility in Cell Imaging. *Angew. Chem., Int. Ed.* **2011**, *50*, 7056−7060.
(41) Rai, S.; Singh, H. Electronic Structure Theory Based Study of Proline Interacting with Gold Nano Clusters. *J. Mol. Model.* **2012**, *10*, 4099−4109.
(42) Rai, S.; Kumar, N. V. S.; Singh, S. A Theoretical Study on Interaction of Proline with Gold Cluster. *Bull. Mater. Sci.* **2012**, *35*, 291−295.
(43) Henzler-Wildman, K.; Kern, D. Dynamic Personalities of Proteins. *Nature (London, U.K.)* **2007**, *450*, 964−972.
(44) Nel, A. E.; Madler, L.; Velegol, D.; Xia, T.; Hoek, E. M. V.; Somasundaran, P.; Klaessig, F.; Castranova, V.; Thompson, M. Understanding Biophysicochemical Interactions at the Nano-Bio Interface. *Nat. Mater.* **2009**, *8*, 543−557.
(45) Hawe, A.; Sutter, M.; Jiskoot, W. Extrinsic Fluorescent Dyes as Tools for Protein Characterization. *Pharm. Res.* **2008**, *25*, 1487−1499.
(46) Maskevich, A. A.; Stsiapura, V. I.; Kuzmitsky, V. A.; Kuznetsova, I. M.; Povarova, O. I.; Uversky, V. N.; Turoverov, K. K. Spectral Properties of Thioflavin T in Solvents with Different Dielectric Properties and in a Fibril-Incorporated Form. *J. Proteome Res.* **2007**, *6*, 1392−1401.
(47) Feng, X. J.; Wu, P. L.; Bolze, F.; Leung, H. W. C.; Li, K. F.; Mak, N. K.; Kwong, D. W. J.; Nicoud, J. F.; Cheah, K. W.; Wong, M. S. Cyanines

as New Fluorescent Probes for DNA Detection and Two-Photon Excited Bioimaging. *Org. Lett.* **2010**, *12*, 2194−2197.
(48) Parasassi, T.; Krasnowska, E.; Bagatolli, L. A.; Gratton, E. Laurdan and Prodan as Polarity-Sensitive Fluorescent Membrane Probes. *J. Fluoresc.* **1998**, *8*, 365−373.
(49) Doye, J. P. K.; Wales, D. J. Global Minima for Transition Metal Clusters Described by Sutton-Chen Potentials. *New J. Chem.* **1998**, *22*, 733−744.
(50) Schneidman-Duhovny, D.; Inbar, Y.; Polak, V.; Shatsky, M.; Halperin, I.; Benyamini, H.; Barzilai, A.; Dror, O.; Haspel, N.; Nussinov, R. Taking Geometry to Its Edge: Fast Unbound Rigid (and Hinge-Bent) Docking. *Proteins* **2003**, *52*, 107−112.
(51) Schneidman-Duhovny, D.; Inbar, Y.; Nussinov, R.; Wolfson, H. J. PatchDock and SymmDock: Servers for Rigid and Symmetric Docking. *Nucl. Acids Res.* **2005**, *33*, 363−367.
(52) Andrusier, N.; Nussinov, R.; Wolfson, H. J. FireDock: Fast Interaction Refinement in Molecular Docking. *Proteins* **2007**, *69*, 139−159.
(53) Mashiach, E.; Schneidman-Duhovny, D.; Andrusier, N.; Nussinov, R.; Wolfson, H. J. FireDock: A Web Server for Fast Interaction Refinement in Molecular Docking. *Nucl. Acids Res.* **2008**, *36*, 229−232.
(54) Berendsen, H. J. C.; van der Spoel, D.; van Drunen, R. GROMACS: A Message-Passing Parallel Molecular Dynamics Implementation. *Comput. Phys. Commun.* **1995**, *91*, 43−56.
(55) Lindahl, E.; Hess, B.; van der Spoel, D. GROMACS 3.0: A Package for Molecular Simulation and Trajectory Analysis. *J. Mol. Model.* **2001**, *7*, 306−317.
(56) Hess, B.; Kutzner, C.; van der Spoel, D.; Lindahl, E. GROMACS 4: Algorithms for Highly Efficient, Load-Balanced, and Scalable Molecular Simulation. *J. Chem. Theory Comput.* **2008**, *4*, 435−447.
(57) Cornell, W. D.; Cieplak, P.; Bayly, C. I.; Gould, I. R.; Merz, K. M.; Ferguson, D. M.; Spellmeyer, D. C.; Fox, T.; Caldwell, J. W.; Kollman, P. A. A Second Generation Force Field for the Simulation of Proteins, Nucleic Acids, and Organic Molecules. *J. Am. Chem. Soc.* **1995**, *117*, 5179−5197.
(58) *Free Energy Calculations: Theory and Applications in Chemistry and Biology*, 1st ed.; Chipot, C., Pohorille, A., Eds.; Springer Series in Chemical Physics; Springer: Berlin, 2007.
(59) Nose, S.; Klein, M. L. Constant Pressure Molecular Dynamics for Molecular Systems. *Mol. Phys.* **1983**, *50*, 1055−1076.
(60) Parrinello, M.; Rahman, A. Polymorphic Transitions in Single-Crystals: A New Molecular Dynamics Method. *J. Appl. Phys.* **1981**, *52*, 7182−7190.
(61) Bussi, G.; Donadio, D.; Parrinello, M. Canonical Sampling through Velocity Rescaling. *J. Chem. Phys.* **2007**, *126*, 14101−14107.
(62) Essmann, U.; Perera, L.; Berkowitz, M. L.; Darden, T.; Lee, H.; Pedersen, L. G. A Smooth Particle Mesh Ewald Method. *J. Chem. Phys.* **1995**, *103*, 8577−8593.
(63) Hess, B.; Bekker, H.; Bendersen, H. J. C.; Fraaije, J. G. E. M. LINCS: A Linear Constraint Solver for Molecular Simulations. *J. Comput. Chem.* **1997**, *18*, 1463−1473.
(64) Humphrey, W.; Dalke, A.; Schulten, K. VMD: Visual Molecular Dynamics. *J. Mol. Graphics* **1996**, *14*, 33−38.
(65) Perdew, J. P.; Burke, K.; Ernzerhof, M. Generalized Gradient Approximation Made Simple. *Phys. Rev. Lett.* **1996**, *77*, 3865.
(66) Perdew, J. P.; Burke, K.; Ernzerhof, M. Errata: Generalized Gradient Approximation Made Simple. *Phys. Rev. Lett.* **1997**, *78*, 1396.
(67) Adamo, C.; Barone, V. Toward Reliable Density Functional Methods without Adjustable Parameters: The PBE0 Model. *J. Chem. Phys.* **1999**, *110*, 6158.
(68) Hay, P. J. Gaussian Basis Sets for Molecular Calculations. The Representation of 3*d* Orbitals in Transition-Metal Atoms. *J. Chem. Phys.* **1977**, *66*, 4377.
(69) Hay, P. J.; Wadt, W. R. Ab Initio Effective Core Potentials for Molecular Calculations. Potentials for the Transition-Metal Atoms Sc to Hg. *J. Chem. Phys.* **1985**, *82*, 270.
(70) Hay, P. J.; Wadt, W. R. Ab Initio Effective Core Potentials for Molecular Calculations. Potentials for K to Au Including the Outermost Core Orbitals. *J. Chem. Phys.* **1985**, *82*, 299.
(71) Norman, P.; Bishop, D. M.; Jensen, H. J. Aa.; Oddershede, J. Nonlinear Response Theory with Relaxation: The First-Order Hyperpolarizability. *J. Chem. Phys.* **2005**, *123*, 194103.
(72) Norman, P.; Bishop, D. M.; Jensen, H. J. Aa.; Oddershede, J. Near-Resonant Absorption in the Time-Dependent Self-Consistent Field and Multiconfigurational Self-Consistent Field Approximations. *J. Chem. Phys.* **2001**, *115*, 10323.
(73) Pedersen, M. N.; Hedegaard, E. D.; Olsen, J. M. H.; Norman, P.; Kongsted, J. Damped Response Theory in Combination with Polarizable Environments: The Polarizable Embedding Complex Polarization Propagator Method. *J. Chem. Theory. Comput.* **2014**, *10*, 1164−1171.
(74) Olsen, J. M.; Aidas, K.; Kongsted, J. Excited States in Solution through Polarizable Embedding. *J. Chem. Theory Comput.* **2010**, *6*, 3721−3734.
(75) Olsen, J. M.; Kongsted, J. Molecular Properties through Polarizable Embedding. *Adv. Quantum Chem.* **2011**, *61*, 107−143.
(76) Kauczor, J.; Jorgensen, P.; Norman, P. On the Efficiency of Algorithms for Solving Hartree−Fock and Kohn−Sham Response Equations. *J. Chem. Theory Comput.* **2011**, *7*, 1610−1630.
(77) Aidas, K.; Angeli, C.; Bak, K. L.; Bakken, V.; Bast, R.; Boman, L.; Christiansen, O.; Cimiraglia, R.; Coriani, S.; Dahle, P.; Dalskov, E. K.; Ekstrom, U.; Enevoldsen, T.; Eriksen, J. J.; et al. The Dalton Quantum Chemistry Program System. *Comput. Mol. Sci.* **2014**, *4*, 269−284.
(78) Yanai, T.; Tew, D.; Handy, N. A New Hybrid Exchange−Correlation Functional Using the Coulomb-Attenuating Method (CAM-B3LYP). *Chem. Phys. Lett.* **2004**, *393*, 51−57.
(79) Dolg, M.; Wedig, U.; Stoll, H.; Preuss, H. Energy-Adjusted Ab Initio Pseudopotentials for the First Row Transition Elements. *J. Chem. Phys.* **1987**, *86*, 866.
(80) Kabsch, W.; Sander, C. Dictionary of Protein Secondary Structure: Pattern Recognition of Hydrogen-Bonded and Geometrical Features. *Biopolymers* **1983**, *22*, 2577−2637.
(81) Balamurugan, K.; Gopalakrishnan, R.; Raman, S. S.; Subramanian, V. Exploring the Changes in the Structure of α-Helical Peptides Adsorbed onto a Single Walled Carbon Nanotube Using Classical Molecular Dynamics Simulation. *J. Phys. Chem. B* **2010**, *114*, 14048−14058.
(82) Balamurugan, K.; Azhagiya Singam, E. R.; Subramanian, V. Effect of Curvature on the α-Helix Breaking Tendency of Carbon Based Nanomaterials. *J. Phys. Chem. C* **2011**, *115*, 8886−8892.
(83) Zuo, G.; Zhou, X.; Huang, Q.; Fang, H.; Zhou, R. Adsorption of Villin Headpiece onto Graphene, Carbon Nanotube, and C60: Effect of Contacting Surface Curvatures on Binding Affinity. *J. Phys. Chem. C* **2011**, *115*, 23323−23328.
(84) Kumagai, I.; Sunada, F.; Takeda, S.; Miura, K. Redesign of the Substrate-Binding Site of Hen Egg White Lysozyme Based on the Molecular Evolution of C-Type Lysozymes. *J. Biol. Chem.* **1992**, *267*, 4608−4612.
(85) Malcom, B. A.; Rosenberg, S.; Corey, M. J.; Allen, J. S.; de Baetselier, A.; Kirsch, J. F. Site-Directed Mutagenesis of the Catalytic Residues Asp-52 and Glu-35 of Chicken Egg White Lysozyme. *Proc. Natl. Acad. Sci. U.S.A.* **1989**, *89*, 133−137.
(86) Inoue, M.; Yamada, H.; Yasukochi, Y.; Kuroki, R.; Miki, T.; Horiuchi, T.; Imoto, T. Multiple Role of Hydrophobicity of Tryptophan-108 in Chicken Lysozyme: Structural Stability, Saccharide Binding Ability, and Abnormal pK_a of Glutamic Acid-35. *Biochemistry* **1992**, *31*, 5545−5553.
(87) Laatikainen, R.; Saarela, J.; Tuppurainen, K.; Hassinen, T. Internal Motions of Native Lysozyme are More Organized Than Those of Mutants: A Principal Component Analysis of Molecular Dynamics Data. *Biophys. Chem.* **1998**, *73*, 1−5.
(88) Cosic, I. The Resonant Recognition Model of Macromolecular Bioactivity, Theory and Applications. *BioMethods* **1997**, *8*, 54.
(89) Mine, S.; Ueda, T.; Hashimoto, Y.; Imoto, T. Analysis of the Internal Motion of Free and Ligand-Bound Human Lysozyme by Use of

^{15}N NMR Relaxation Measurement: A Comparison with Those of Hen Lysozyme. *Protein Sci.* **2000**, *9*, 1669−1684.
(90) Mine, S.; Tate, S. I.; Ueda, T.; Kainosho, M.; Imoto, T. Analysis of the Relationship between Enzyme Activity and its Internal Motion using Nuclear Magnetic Resonance: ^{15}N Relaxation Studies of Wild-type and Mutant Lysozyme. *J. Mol. Biol.* **1999**, *286*, 1547−1565.
(91) Ohmura, T.; Motoshima, H.; Ueda, T.; Imoto, T. Fluctuations in Free or Substrate-Complexed Lysozyme and a Mutant of It Detected on X-Ray Crystallography and Comparison with Those Detected on NMR. *J. Biochem.* **2002**, *131*, 701−704.
(92) Goel, S.; Velizhanin, K. A.; Piryatinski, A.; Ivanov, S. A.; Tretiak, S. Ligand Effects on Optical Properties of Small Gold Clusters: A TDDFT Study. *J. Phys. Chem. C* **2012**, *116*, 3242−3249.
(93) Devadas, M. S.; Bairu, S.; Qian, H.; Sinn, E.; Jin, R.; Ramakrishna, G. Temperature-Dependent Optical Absorption Properties of Monolayer-Protected Au_{25} and Au_{38} Clusters. *J. Phys. Chem. Lett.* **2011**, *2*, 2752−2758.
(94) Muhammed, M. A. H; Pradeep, T. Au_{25}@SiO_2: Quantum Clusters of Gold Embedded in Silica. *Small* **2011**, *7*, 204−208.
(95) Fihey, A.; Maurel, F.; Perrier, A. Modeling the Absorbance Properties of a Pyrene Chromophore Grafted onto a Au_{25} Nanocluster: A TD-DFT Study. *J. Phys. Chem. C* **2014**, *118*, 4444−4453.
(96) Mathew, A.; Natarajan, G.; Lehtovaara, L.; Hakkinen, H.; Kumar, R. M.; Subramanian, V.; Jaleel, A.; Pradeep, T. Supramolecular Functionalization and Concomitant Enhancement in Properties of Au_{25} Clusters. *ACS Nano* **2014**, *8*, 139−152.
(97) Negishi, Y.; Kurashige, W.; Kamimura, U. Isolation and Structural Characterization of an Octaneselenolate-Protected Au_{25} Cluster. *Langmuir* **2011**, *27*, 12289−12292.
(98) Song, Y.; Zhong, J.; Yang, S.; Wang, S.; Cao, T.; Zhang, J.; Li, P.; Hu, D.; Pei, Y.; Zhu, M. Crystal Structure of $Au_{25}(SePh)_{18}$ Nanoclusters and Insights into Their Electronic, Optical and Catalytic Properties. *Nanoscale* **2014**, *6*, 13977−13985.
(99) Muhammed, M. A. H.; Pradeep, T. Aqueous to Organic Phase Transfer of Au_{25} Clusters. *J. Clust Sci.* **2009**, *20*, 365−373.
(100) Zhu, M.; Aikens, C. M.; Hollander, F. J.; Schatz, G. C.; Jin, R. Correlating the Crystal Structure of a Thiol-Protected Au_{25} Cluster and Optical Properties. *J. Am. Chem. Soc.* **2008**, *130*, 5883−5885.